# EUROPEAN ORGANIZATION FOR NUCLEAR RESEARCH

# D*±mesons in jets in p–Pb collisions: preliminary figures for EPS and SQM 2017

Salvatore Aiola[1], Fabio F. Colamaria[2], Andrea Rossi[3], Antonio C. O. da Silva[4,5], Barbara A. Trzeciak[4]

1. Yale University, USA
2. University of Bari and INFN, Italy
3. University of Padova and INFN, Italy
4. Utrecht University, Netherlands
5. University of São Paulo, Brazil

Email: barbara.antonina.trzeciak@cern.ch

## Abstract

The study of the charm content of jets is interesting because up to now it has eluded a precise quantitative understanding in the framework of perturbative QCD (pQCD). The charm content of jets is known to arise both from prompt production in the process $gg(q\bar{q}) \to c\bar{c}$, and from the parton shower of gluons and light-flavor quarks. Charm hadrons coming from the fragmentation of prompt charm jets are expected to carry a larger fraction of the total jet momentum, as compared to those where the charm content arises later in the parton shower. Therefore the measurement of charm jet fragmentation functions (FFs) can be used to estimate the relative strength of the two mechanisms. Heavy-flavor jets can also provide important insights into the Quark-Gluon Plasma (QGP) produced in ultra-relativistic heavy-ion collisions, as heavy quarks are predicted to interact with the QGP differently compared to light quarks and gluons. The aim of the analysis is to extract both the $p_T$ spectrum of the D-tagged jets and the jet-momentum fraction of the D mesons. We identify D-meson candidates via their hadronic decay channels using topological selections and particle identification. These D-meson candidates are combined with the other charged tracks reconstructed by the central tracking system, using the anti-$k_T$ jet-finding algorithm. We extract the yield of D-tagged jets through an invariant mass analysis of the D-meson candidates associated with each jet, in bins of jet $p_T$ and momentum fraction carried by the D meson. At the Strangeness in Quark Matter 2017 conference we show new preliminary results from the p–Pb analysis. These results include solely th $p_T$ spectrum of the D-tagged jets.

## Contents

## 1   Software

The main analysis tasks (`C++` classes) used in the analysis are in the `PWGJE` library of the `AliPhysics` software package:

- `AliAnalysisTaskSEDmesonsFilterCJ` (filters D mesons and create a set of particles with the D meson instead of the daughters);

- `AliAnalysisTaskFlavourJetCorrelations` (correlates each found D meson with a jet);

- `AliEmcalJetTask`;

- `AliAnalysisTaskRhoSparse`.

The `AliPhysics` version used for this analysis is the analysis tag: `vAN-20170517` (with `AliRoot v5-09-06-1`).

The task used for this analysis generates a multiple axis histogram (`THnSparse`) that keep informations about: $z_{||}$, jet $p_T$, D-meson $p_T$ and D-meson invariant mass.

The post-processing includes: projection of the `THnSparse` into lower-dimensional histograms, raw signal extraction, response matrix generation, unfolding, B feed-down correction and the final plotting. The post-processing is relatively light-weight and is performed directly in a personal computer. This code is written using the `C++` with `ROOT`.

## 2   Dataset and Event Selection

For this analysis we use the data collected by ALICE in 2016 during the Minimum Bias period of the p–Pb collisions at $\sqrt{s_{NN}} = 5.02$ TeV. These data corresponds to the following data taking periods: LHC16q and LHC16t pass1, FAST and CENT_woSDD productions were merged, the total number of events is 561.1 M (after all the selections outlined below) out of 825.6 M analysed. The complete list of runs used in this analysis is:

LHC16q: 265525, 265521, 265501, 265500, 265499, 265435, 265427, 265426, 265425, 265424, 265422, 265421, 265420, 265419, 265388, 265387, 265385, 265384, 265383, 265381, 265378, 265377, 265344, 265343, 265342, 265339, 265338, 265336, 265335, 265334, 265332, 265309
LHC16t: 267166, 267165, 267164, 267163

Events were selected using the event selection `kINT7`. Note that the analysis is performed in `AOD`, where the beam-gas and gas-gas events have been filtered out. Events were further filtered using the Physics Selection, and selection provided by:

- `AliAnalysisTaskEmcal::IsEventSelected()`, which rejects events based on event vertex quality, in particular requiring a reconstructed vertex position not farther than 10 cm from the center of the detector along the beam axis; and a distance between the SPD vertex and the V0 vertex not larger than 0.5 cm

- `AliRDHFCutsDStartoKpipi::IsEventSelected(AliVEvent*)`, which rejects events based on event vertex quality and pileup

Results shown below come from the LEGO trains HFCJ_pPb:
188 (LHC16q_pass1_FAST), 189 (LHC16q_pass1_CENT_woSDD), 190 ( LHC16t_pass1_FAST) and 191 (LHC16t_pass1_CENT_woSDD).

### 2.0.1 *Monte Carlo productions*

For this analysis the Monte Carlo production LHC17d2a_fast_new has been used, anchored to the 2016 p–Pb data taking periods LHC16q and LHC16t and the FAST production. The FAST production simulation is used to corrected the datasample, which is merged FAST+CENT_woSDD, assuming that efficiencies are detector response are the same for both. The simulations uses PYTHIA6 with the Perugia2011 tune as particle generator at $\sqrt{s} = 5.02$ TeV. If $N_{coll} > 1$, the even generated by Hijing is also embedded. The charm content has been enhanced by requesting a $c\bar{c}$ in 50% of the events and a $b\bar{b}$ in the remaining half. Furthermore, all D mesons are forced to decay hadronically. This MC production is used to compute the D-meson efficiency with jets, acceptance corrections and a response matrix of D-tagged jets with prompt and non-prompt $D^{*\pm}$: $c, b \rightarrow D^{*\pm}$.

## 3   D-Meson Selection

The $D^{*\pm}$mesons were reconstructed through their hadronic decay channels [**?**]:

$$D^{*\pm} \rightarrow D^0 + \pi^\pm \rightarrow K^\pm + \pi^\mp + \pi^\pm \text{ , BR} = 67.7\pm0.5\%, 3.93\pm0.04\%$$

The selection strategy is based on the topological displacement of the secondary vertex from the primary vertex due to their relatively large lifetime.

The candidate vertices are read from the AOD friend chain `AliAOD.VertexingHF.root`. A list of topological and kinematic cuts applied for $D^{*\pm}$ in p–Pb collisions at $\sqrt{s_{NN}} = 5.02$ TeV can be found in Table 1. The same quality track selection on the decay products used for the D-meson spectra analysis of the same datasets has been used in this analysis. D mesons are required to have $1 < p_{T,D} < 36$ GeV/$c$, while for the final jet spectrum we will apply $p_{T,D} > 3$ GeV/$c$ on the D mesons. The accepted $|y_D|$ range is $p_T$-dependent, with the upper limit growing from 0.5 to 0.8 at $p_T = 5$ GeV/$c$.

Table 1: $D^{*\pm}$ cuts for p–Pb collisions at $\sqrt{s_{NN}} = 5.02$ TeV.

| $p_{T,D^0}$ (GeV/$c$) | $0.5-1$ | $1-2$ | $2-3$ | $3-4$ | $4-5$ | $5-6$ | $6-7$ | $7-8$ | $8-10$ | $10-12$ | $12-16$ | $16-24$ | $24-36$ |
|---|---|---|---|---|---|---|---|---|---|---|---|---|---|
| $\Delta M_{D^0}$ (GeV/$c^2$) | 0.03 | 0.032 | 0.032 | 0.032 | 0.032 | 0.036 | 0.036 | 0.036 | 0.05 | 0.05 | 0.094 | 0.094 | 0.7 |
| DCA (cm) | 0.0315 | 0.025 | 0.03 | 0.03 | 0.035 | 0.04 | 0.08 | 0.12 | 0.12 | 0.12 | 0.2 | 0.2 | 0.5 |
| $\cos(\theta^*)$ | 0.9 | 0.8 | 0.8 | 0.8 | 0.9 | 1 | 1 | 1 | 1 | 1 | 1 | 1 | 1 |
| $p_{T,K}$ (GeV/$c$) | 0.5 | 1 | 1 | 1 | 1 | 1 | 1 | 1 | 1 | 1 | 0.3 | 0.3 | 0 |
| $p_{T,\pi}$ (GeV/$c$) | 05 | 1 | 1 | 1 | 1 | 1 | 1 | 1 | 1 | 1 | 0.3 | 0.3 | 0 |
| $d_0^K$ (cm) | 0.1 | 0.1 | 0.1 | 0.1 | 0.1 | 0.1 | 0.1 | 0.1 | 0.1 | 0.1 | 0.2 | 0.2 | 999 |
| $d_0^\pi$ (cm) | 0.1 | 0.1 | 0.1 | 0.1 | 0.1 | 0.1 | 0.1 | 0.1 | 0.1 | 0.1 | 0.2 | 0.2 | 999 |
| $d_0^K \cdot d_0^\pi$ ($10^{-4}$cm$^2$) | -3 | -2 | -2.5 | -1.3 | -0.38 | 0.44 | 5 | 5 | 100 | 100 | 500 | 1000 | 1000 |
| $\cos(\theta_{point})$ | 0.8 | 0.9 | 0.9 | 0.87 | 0.86 | 0.83 | 0.76 | 0.76 | 0.68 | 0.68 | 0.85 | -1 | -1 |
| $\cos(\theta_{point,xy})$ | - | 0.97 | - | - | - | - | - | - | - | - | - | - | - |
| $L_{xy}$(cm) | 4 | 3.5 | 4 | 3.5 | 3 | 2.5 | 1.5 | 1 | 0 | 0 | 0 | 0 | 0 |

### 3.1   Particle Identification

The Particle Identification (PID) of pions and kaons was performed using the information of the specific energy loss in the TPC and the time of flight provided by the TOF detector. In order to identify a track as a pion or a kaon its TPC d$E$/d$x$ and/or time-of-flight were required to be within $3\sigma$ of the expected values. Tracks with no TOF information were identified using only the TPC. Tracks compatible with both the kaon and the pion hypotheses were retained for analysis and both mass hypotheses were considered.

## 4    Jet Reconstruction

The FASTJET[?] package was used to reconstruct the jets. In particular, the anti-$k_T$ algorithm [?] was employed to reconstruct signal jets. This algorithm is infrared-safe (not sensitive to low energy radiations) and collinear-safe (not sensitive to collinear particle splitting). A resolution parameter of $R = 0.4$ was used for both the p–Pb analyses. In the p–Pb analysis, the $k_T$ algorithm [?] was employed to estimate the background. For this analysis, only charged tracks are used to reconstructed the jets (*charged jets*).

The set of tracks given as input to the jet finder has the D-meson daughters replaced by the 4-momentum of the D-meson candidate (sum of the 4-momenta of the daughters). The procedure is repeated independently for each D-meson candidate in each event, i.e. each candidate is treated as if it was the only one in the event, then (if there is more than one candidate) the procedure is repeated for each candidate one by one. This is done because two (or even more) candidates can share the same daughter.

### 4.1    Jet Selection

Tracks with $p_T > 0.15$ GeV/$c$ and $|\eta| < 0.9$ were included in the jet finding. Reconstructed jets with the axis not satisfying $|\eta_{\text{jet}}| < 0.9 - R$ were rejected.

## 5    Raw Yield Extraction

We have implemented two methods to extract the D-tagged jet $p_T$ distribution. The D\*± the fit is performed using a Gaussian distribution for the signal and the following function for the background:

$$f_{\text{bkg}}(m) = a(m - m_\pi)^{0.5} \exp(b(m - m_\pi)), \tag{1}$$

where $m$ is the invariant mass, $a$ and $b$ are free parameters of the fit.

**Invariant mass fit in jet $p_T$ bins**    The invariant mass distribution of the D-meson candidates is built for each $p_{T,\text{chjet}}$ bin and the signal is extracted directly from the fit parameters.

**Side-band subtraction in D-meson $p_T$ bins**    The invariant mass distribution of the D-meson candidates is built for each $p_{T,D}$ bin and the D-meson candidates that belongs to the bins in the signal region ($3\sigma$ around the peak position) are used to build the peak-region jet $p_T$ distribution; in order to remove the contribution of D-meson background, the jet $p_T$ distribution corresponding to the side-band region (between $-8\sigma$ and $-5\sigma$ from the left-hand side of the D\*± peak and between $5\sigma$ and $13\sigma$ on the right-hand side) is taken and normalized to the background integral in the signal region, estimated from the fit.

### 5.1    Invariant Mass Fit Method

The D-meson invariant mass is analyzed for each bin of jet $p_T$. The D-tagged jet raw yield and its uncertainty are extracted from the integral of the Gaussian fit function in the signal region. The invariant mass distributions in bins of jet $p_T$ are shown in Fig. 1.

Figure 2 shows a summary of the raw signal extraction: yield, relative statistical uncertainty, signal / background ratio and significance.

The invariant mass distributions shown here are not corrected for the reconstruction efficiency. This step is discussed in Sec. 6.1.

The jet $p_T$ bins are selected so that the significance of the D signal is above $5\sigma$. The final jet $p_T$ range for the p–Pb analysis is $4 < p_T < 40$ GeV/$c$. The reason of the D\*± signal visible in the Fig. 1 below $p_{T,\text{jet}}$ of 3 GeV/$c$ despite the $p_{T,D}$ cut above 3 GeV/$c$ is a subtraction of the jet background, as it is described in the Sec. 8.1.
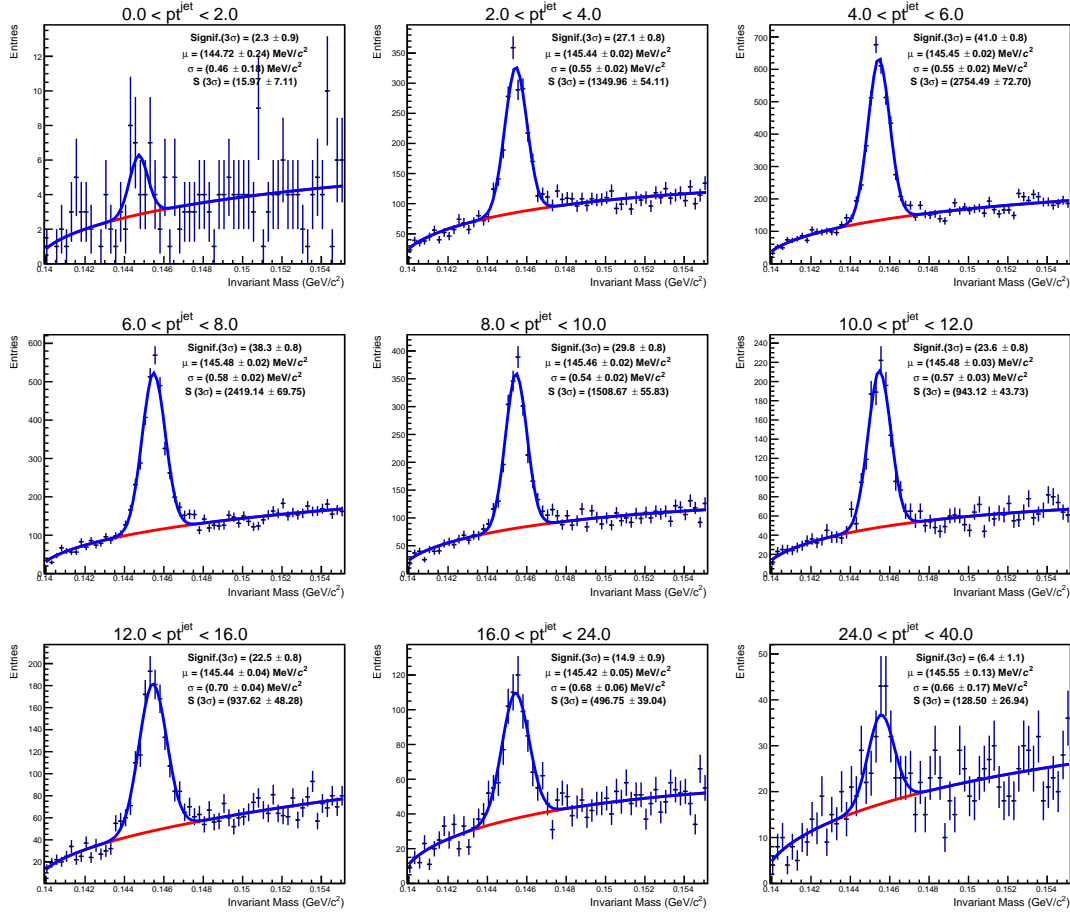
Fig. 1: D$^{*\pm}$-jet signal extraction in bins of jet transverse momentum in p–Pb collisions at $\sqrt{s_{NN}} = 5.02$ TeV (raw yields). D mesons are required to have $p_T > 3$ GeV/$c$.

## 5.2 Side-Band Subtraction Method

The D-meson invariant mass is analyzed for each bin of D-meson $p_T$. The D-meson candidates in the signal region are used to build a jet $p_T$ distribution, which comprises both signal and background D-meson candidates. Another jet $p_T$ distribution is built using candidates with invariant mass that is between $-8\sigma$ and $-5\sigma$ from the left-hand side of the D$^{*\pm}$ peak and between $5\sigma$ and $13\sigma$ on the right-hand side. The normalization is done using the information of the fit integrating the background function inside the signal area. This is done separately and independently for each $p_{T,D}$ bin.

The invariant mass distributions in bins of D-meson $p_T$ are shown in Fig. 3.

For p–Pb the signal region is defined as $3\sigma$ around the peak and is shown as the red shadow area in Fig. 3; the background region, $5\sigma$ away from the peak mean position, is depicted as the blue area in Fig. 3.

The jet $p_T$ distributions are shown in Fig. 4, along with the jet distributions for the background region. Then the background distributions are subtracted from the signal distributions and raw jet $p_T$ distributions are obtained in each D $p_T$ bin, as is it shown also in Fig. 4. Figure 5 shows the sum of the jet $p_T$ distributions for D$^{*\pm}$-jets without a correction for the D meson efficiency and rebinning.

Figure 6 shows a summary of the raw signal extraction: yield, relative statistical uncertainty, signal / background ratio and significance.

In order to obtain the final jet $p_T$ spectrum, the distributions in each D $p_T$ bin need to be corrected for the D efficiency and finally summed up. The corrections will be discussed in Section 6.1.
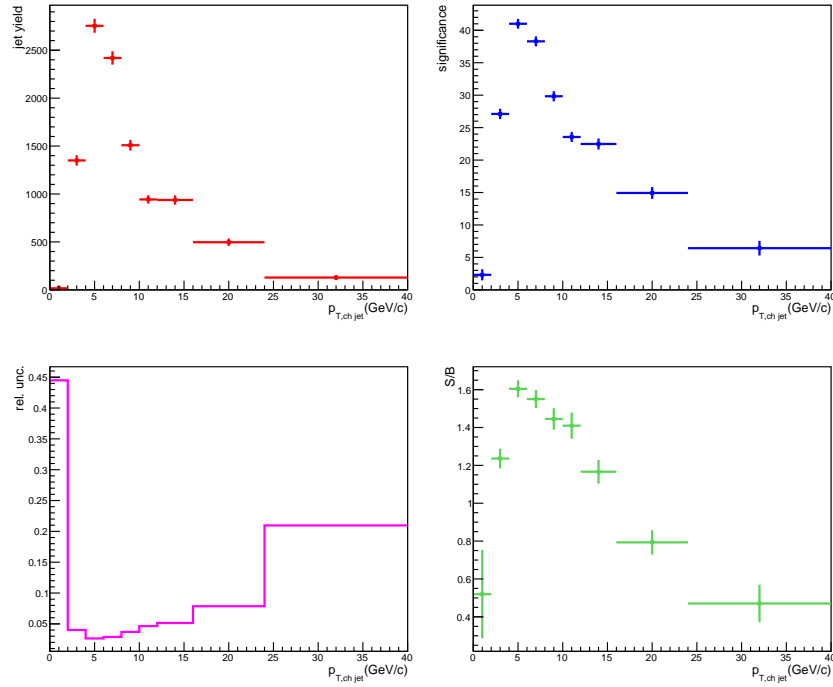
Fig. 2: D*±-jet raw signal extraction in p–Pb collisions at $\sqrt{s} = 5.02$ TeV for $p_{T,D} > 3$ GeV/$c$ with the invariant mass fit method in bins of $p_{T,\text{ch jet}}$.

## 5.3 Method Comparison

Figure 7 shows a comparison of the raw yields (without the D-reconstruction efficiency applied). Jets spectra are checked with two cuts on the D-meson $p_T$: $p_{T,D} > 2$ GeV/$c$ and $p_{T,D} > 3$ GeV/$c$. Both agree with each other as it is seen in Fig. 7. However, it is more important to cross-check the two methods with different $p_{T,D}$ cuts after the efficiency correction is applied, as the background at low $p_{T,D}$ influences the analysis more, as it is shown later.
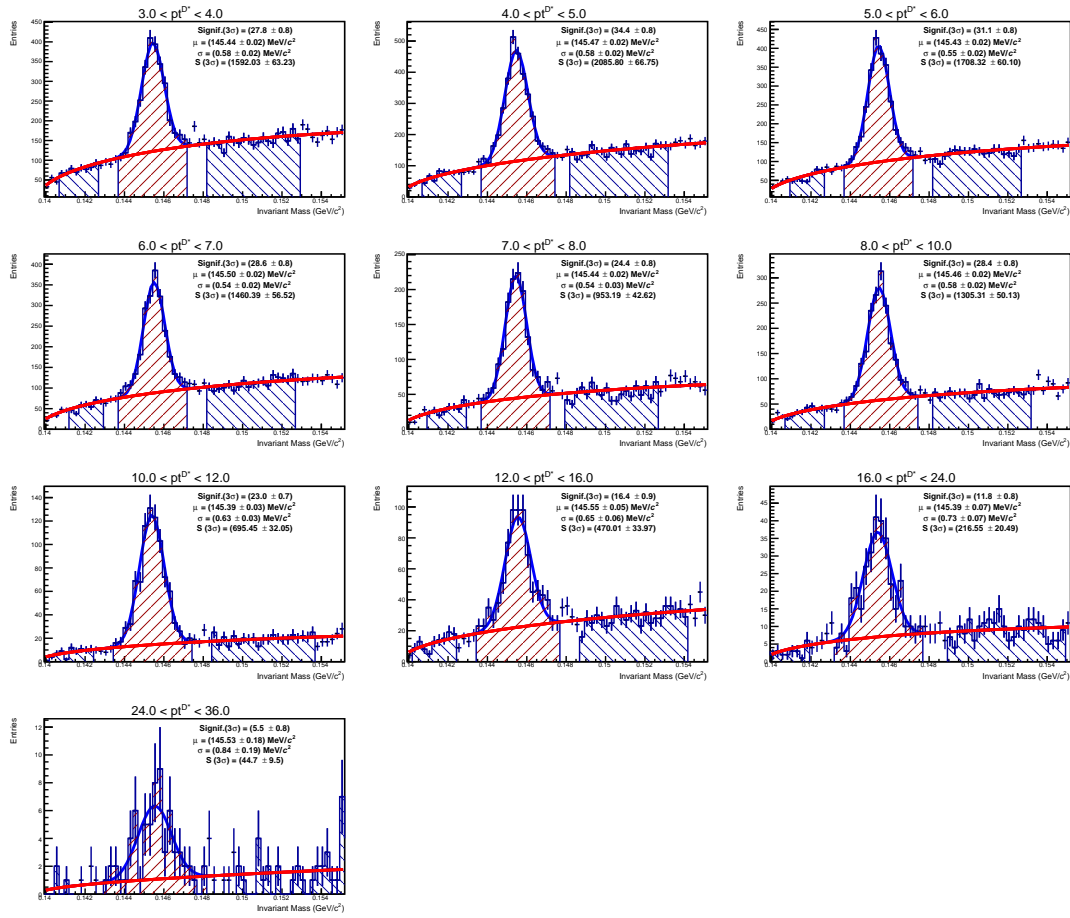
Fig. 3: $D^{*\pm}$ signal extraction in bins of D-meson transverse momentum in p–Pb collisions at $\sqrt{s_{\mathrm{NN}}} = 5.02$ TeV (raw yields).
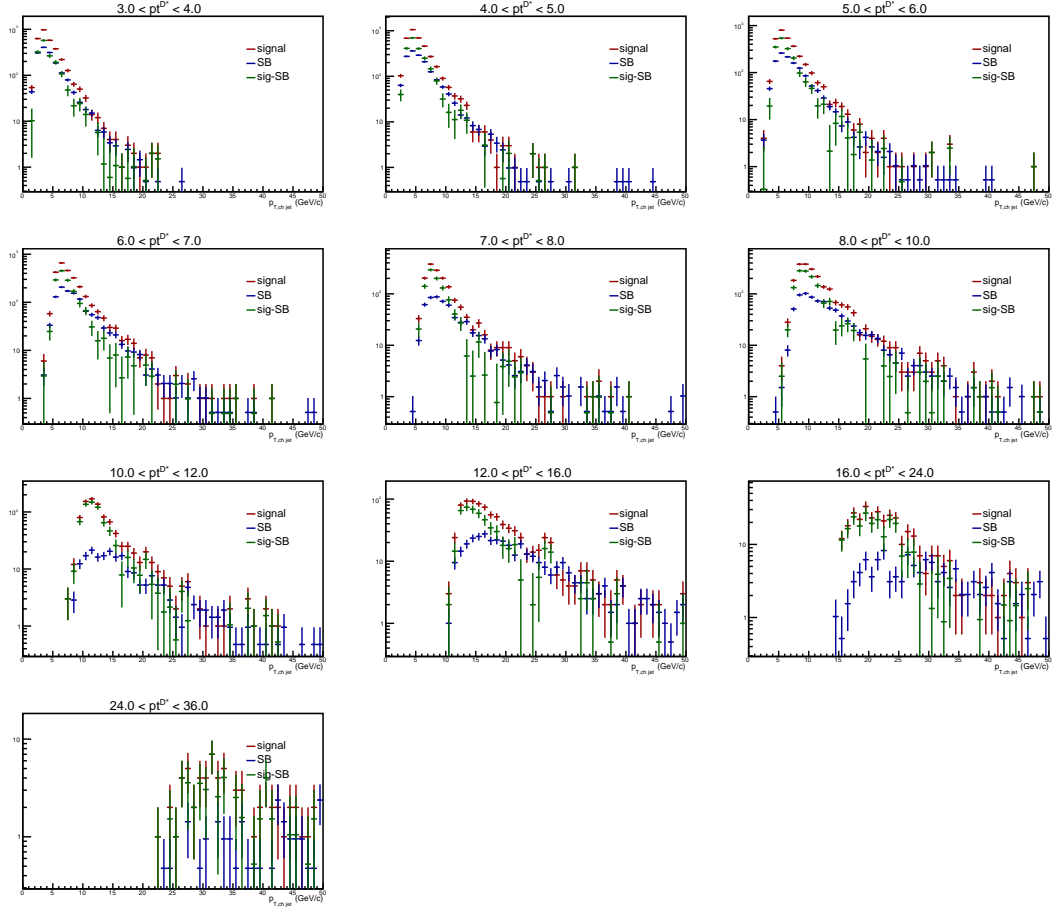
Fig. 4: Raw jet $p_{\mathrm{T}}$ distributions in bins of D-meson transverse momentum in p–Pb collisions at $\sqrt{s_{\mathrm{NN}}} = 5.02$ TeV.
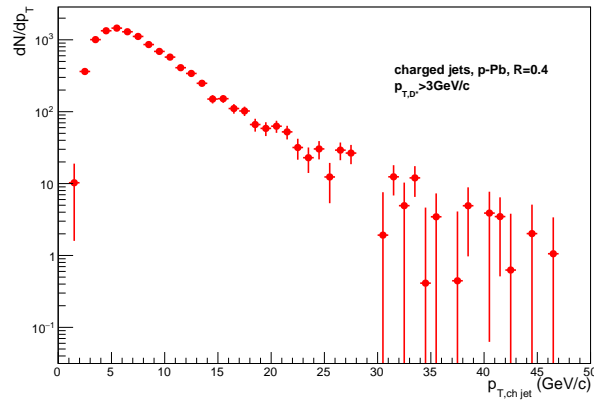


Fig. 5: Total raw jet $p_{\mathrm{T}}$ distributions in p–Pb collisions at $\sqrt{s_{\mathrm{NN}}} = 5.02$ TeV, obtained summing together all the D$^{*\pm}$ $p_{\mathrm{T}}$ bins.
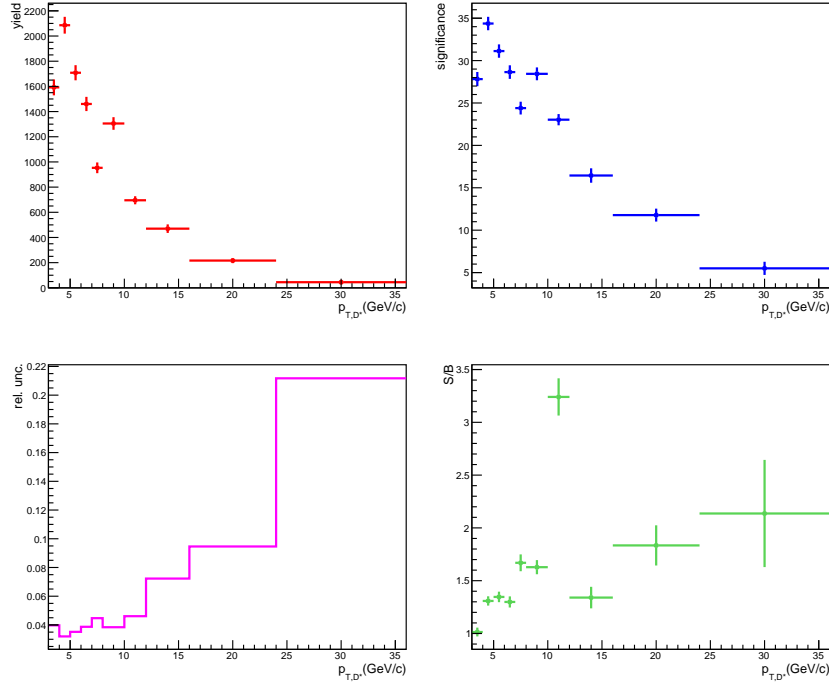
Fig. 6: D$^{*\pm}$-jet raw signal extraction in p–Pb collisions at $\sqrt{s} = 5.02$ TeV for $p_{\mathrm{T,D}} > 3$ GeV/$c$ with the Side Band method.



(a) Yields, $p_{\mathrm{T,D}} > 2$ GeV/$c$

(b) Yields, $p_{\mathrm{T,D}} > 3$ GeV/$c$

(c) Ratio, $p_{\mathrm{T,D}} > 2$ GeV/$c$
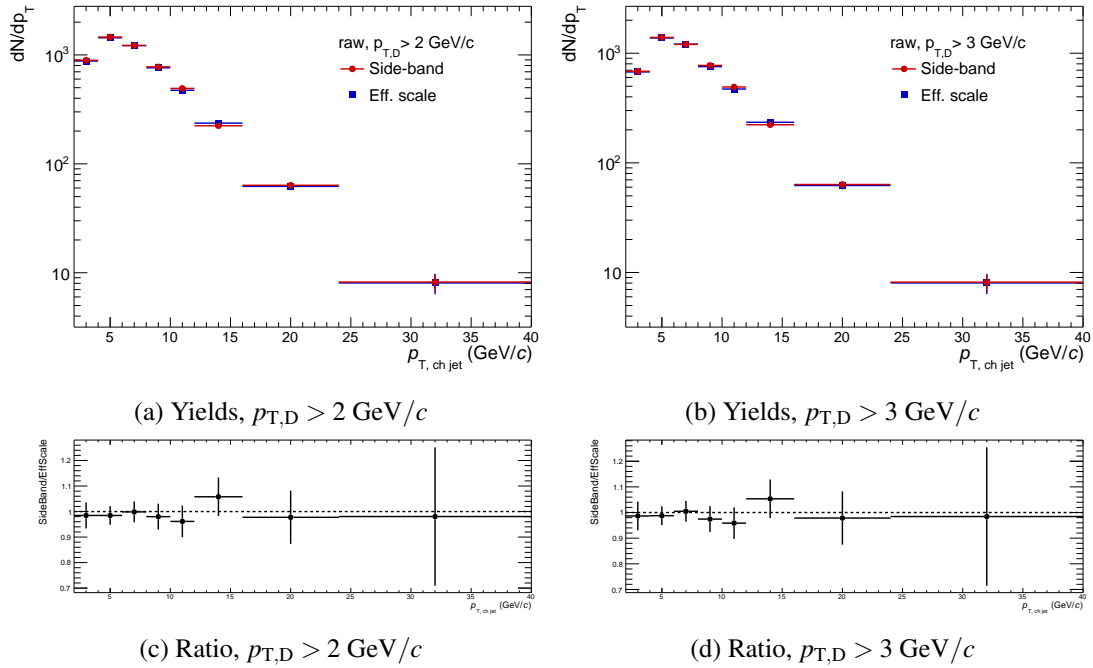
(d) Ratio, $p_{\mathrm{T,D}} > 3$ GeV/$c$

Fig. 7: Comparison of the raw yields obtained using the invariant mass fit method and the side band method without the efficiency correction for D$^{*\pm}$-jets in p–Pb collisions at $\sqrt{s} = 5.02$ TeV with $p_{\mathrm{T,D}} > 2$ GeV/$c$(left) and $p_{\mathrm{T,D}} > 3$ GeV/$c$(right).

## 6  Efficiency Correction Procedure

### 6.1  Reconstruction Efficiency

The efficiency and acceptance (Acc × $\varepsilon$) were calculated using Monte Carlo PYTHIA6+GEANT3 simulations anchored to the data.

The efficiency is taken as the ratio of the $p_{T,D}$ spectra of the D-tagged generator-level jets for which a matched D-tagged detector-level jet was found over all the generated D-tagged jets. For the detector-level jets, the D meson is required to be within the standard fiducial rapidity cuts. Jets are further requested to have $|\eta_{jet}| < 0.9 - R$, both at generator and detector levels.



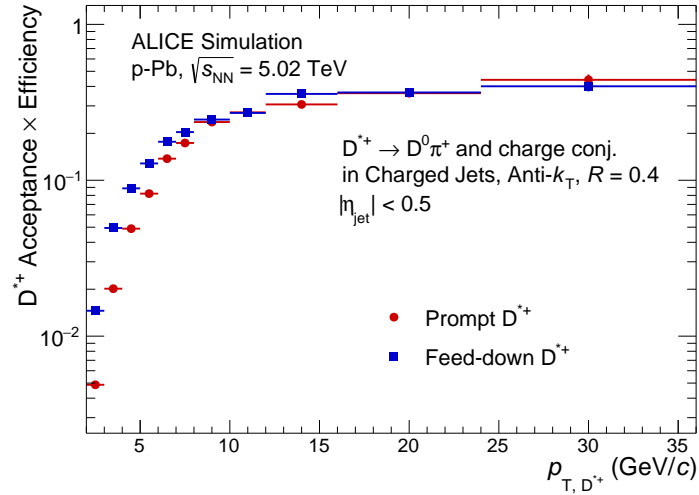Fig. 8: D*± reconstruction efficiency in p–Pb collisions at $\sqrt{s_{NN}} = 5.02$ TeV, for prompt D* in red and non-prompt in blue.

Figure 8 shows the D*± reconstruction efficiency as a function of $p_{T,D}$ for prompt and non-prompt D*±. The efficiency depends strongly on $p_{T,D}$ because of the topological cuts that are relaxed at higher momenta where the combinatorial background is smaller.

### 6.2  Efficiency-Corrected Yields

As discussed in the previous Section, the D-meson reconstruction efficiency shows a strong dependence on $p_{T,D}$(but has very weak or no dependence on $p_{T,jet}$). Therefore, in order to reduce the dependence on the Monte Carlo simulation for what concerns jet fragmentation and momentum spectral shape, the efficiency should be applied as a function of the D-meson momentum. In fact, each bin of $p_{T,jet}$ has contributions from D mesons with very different $p_{T,D}$, which have different efficiencies.

The efficiency-rescaling procedure of the invariant mass distribution $M(p_{T,jet}, p_{T,D})$ was implemented according to the following formula:

$$M(p_{T,jet}) = \sum_{p_{T,D}} \frac{M(p_{T,jet}, p_{T,D})}{(Acc \times \varepsilon)_{p_{T,D}}}. \qquad (2)$$

Figure 10 shows the invariant mass distributions for different ranges of $p_{T,chjet}$, after the efficiency reweighing procedure.

In the side-band method the efficiency is applied by rescaling by $1/(Acc \times \varepsilon)$ the jet $p_T$ spectra in each D-meson $p_T$ bin shown in Fig. 4. The background subtracted distributions are summed up to obtain the corrected jet $p_T$ spectrum. The efficiency corrected spectrum is shown in Fig. **??**
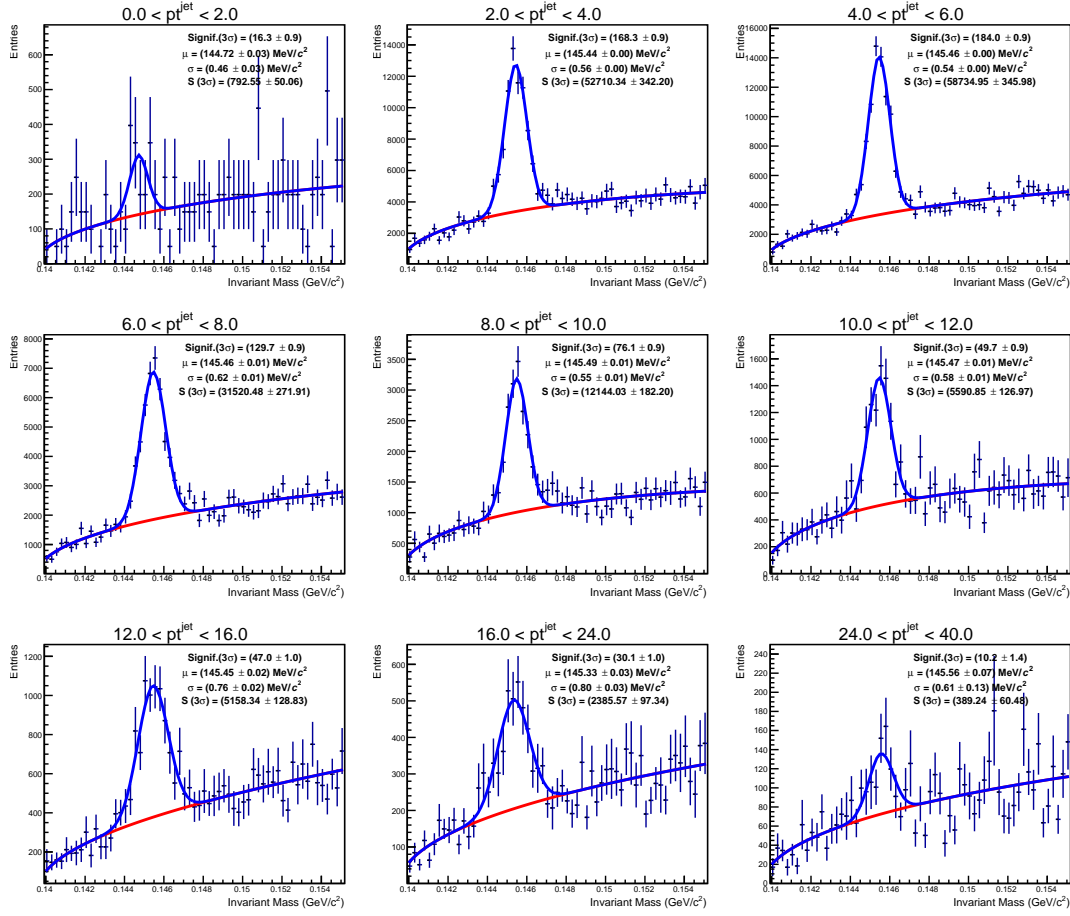
Fig. 9: D$^{*\pm}$ signal extraction in bins of jet transverse momentum in p–Pb collisions at $\sqrt{s_{NN}} = 5.02$ TeV. D mesons are required to have $p_{T,D} > 3$ GeV/$c$. Each candidate is weighted by the inverse of the reconstruction efficiency, which depends on its $p_{T,D}$.

The efficiency corrected jet $p_T$ spectra for both methods with the same binning are shown below.

## 6.3    Method Comparison (Efficiency-Corrected Yields)

Figure 11 shows a comparison of the efficiency-corrected yields obtained using the invariant mass method and the side band method for D$^{*\pm}$-jets with $p_{T,D} > 2$ GeV/$c$ and $p_{T,D} > 3$ GeV/$c$. As mentioned before, the invariant mass method is sensitive to weighing with low efficiency, low $p_T$ D* mesons. Therefore, discrepancies for higher $p_{T,jet}$ ranges between two methods are visible with $p_{T,D} > 2$ GeV/$c$ cut. With $p_{T,D} > 3$ GeV/$c$ cut the two methods agree very well with each other within the statistical uncertainties. Figure 12 shows relative statistical uncertanties for the Side-Band subtraction method with $p_{T,D} > 2$ GeV/$c$ and $p_{T,D} > 3$ GeV/$c$; $p_{T,D} > 3$ GeV/$c$ cut reduces also uncertainties on the jet spectra for higher $p_{T,jet}$.

The default method used for the further analysis is the Side Band method with $p_{T,D} > 3$ GeV/$c$ cut. The method is more stable, Gaussian fits perform better when they are done in $p_{T,D}$ bins, and it is easier to perform the jet spectra analysis with more fine binning if needed.
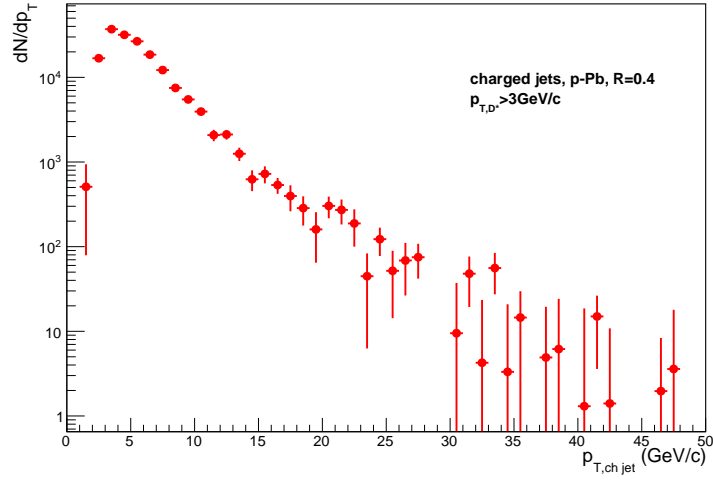
Fig. 10: Efficiency corrected D*±-jets yield obtained for the Side-Band subtraction method in p–Pb collisions at $\sqrt{s_{NN}} = 5.02$ TeV. D mesons are required to have $p_{T,D} > 3$ GeV/$c$.



(a) Yields



(b) Yields



(c) Ratio



(d) Ratio
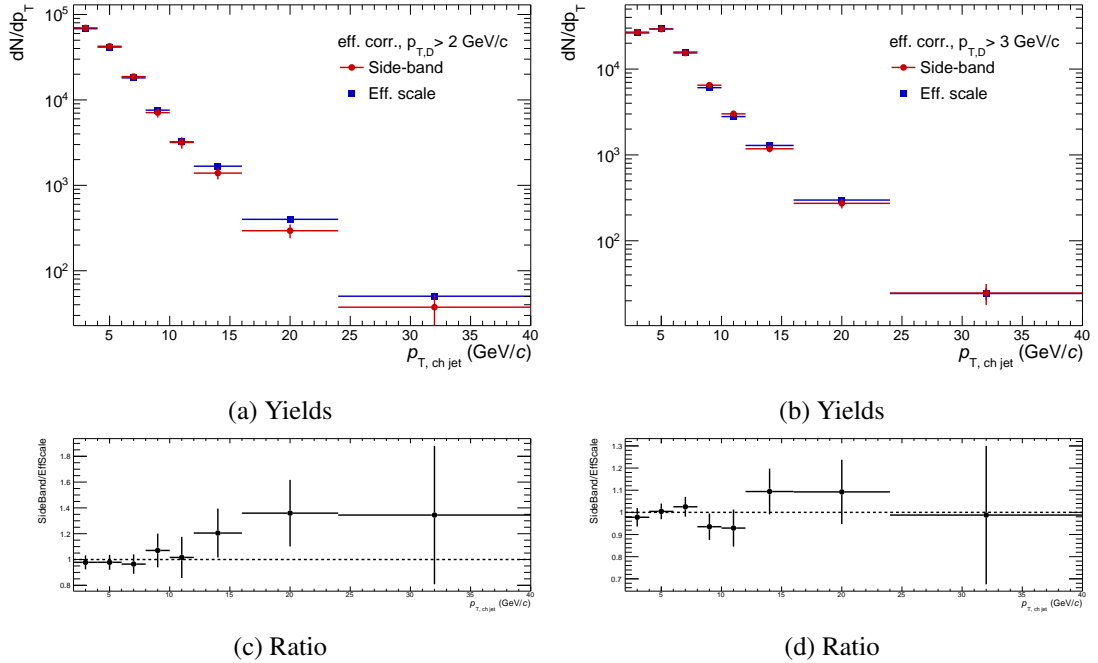
Fig. 11: Comparison of the yields obtained using the invariant mass fit method and the side band method for D*±-jets in p–Pb at $\sqrt{s_{NN}} = 5.02$ TeV, with two cuts on $p_{T,D}$: $p_{T,D} > 2$ GeV/$c$ and $p_{T,D} > 3$ GeV/$c$. Reconstruction efficiency correction is applied in both cases.

Fig. 12: Comparison of the statistical uncertainties obtained using the side band method for D$^{*\pm}$-jets in p–Pb at $\sqrt{s_{\mathrm{NN}}} = 5.02$ TeV, with two cuts on $p_{\mathrm{T,D}}$: $p_{\mathrm{T,D}} > 2$ GeV/$c$ (left) and $p_{\mathrm{T,D}} > 3$ GeV/$c$ (right). Reconstruction efficiency correction is applied in both cases.
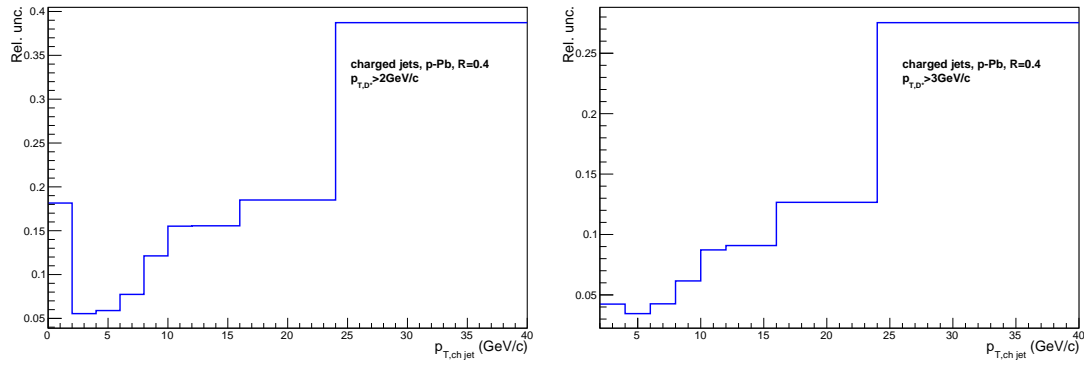
## 7 Jet Momentum Detector Response

The detector response is studied with a Monte Carlo simulation in which particles generated by an event generator are run through a transport code (GEANT3), that simulates the response of the detector elements, and then the same event reconstruction used in data is performed. Only $c\bar{c}$ events are used.

Two sets of jets are obtained from the same event. One of them is obtained from the generator-level information and the second from the reconstructed signals after the detector simulation. The generated and reconstructed jets are matched by looking for the same D meson at both levels (using its MC label).

### 7.1 Response Matrix

The detector response matrix for prompt D*-jets is shown in Fig. 13. Only PYTHIA part of the simulation is The Monte Carlo production is with Hijing. However, in order to avoid Hijing imperfection of describing the underlying event, only the Pythia part of the production is used to extract the detector response matrix, and the background fluctuations matrix is obtained from data 8.2.
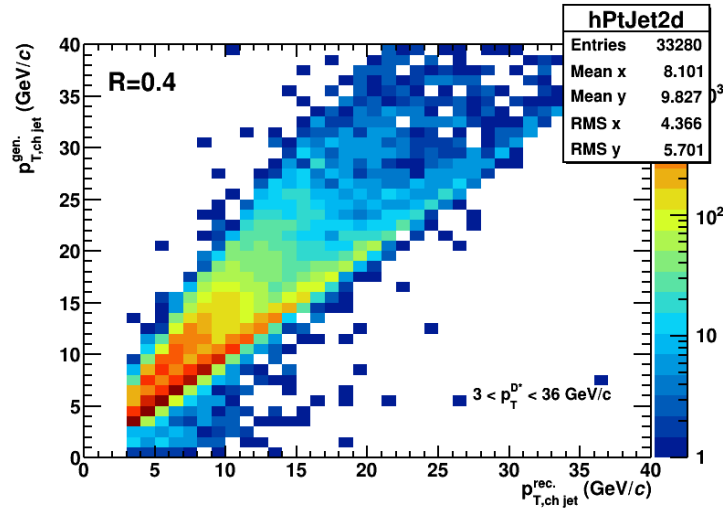


Fig. 13: Detector response matrix calculated with a full simulation of p–Pb events at $\sqrt{s_{NN}} = 5.02$ TeV.

## 8 Underlying Event (p–Pb analysis)

### 8.1 Average Background Momentum Density

The Underlying Event (UE) affects the reconstructed jet momentum and need to be subtracted. The average background density $\rho$ is calculated on an event-by-event basis:

$$\rho_{p-Pb} = \text{median} \left\{ \frac{p_{T,jet}^{k_T}}{A_{jet}^{k_T}} \right\} C. \tag{3}$$

where $p_{T,jet}^{k_T}$ and $A_{jet}^{k_T}$ are respectively the area and the transverse momentum of the jets found using the $k_T$ algorithm. The jet area is estimated by FASTJET using the active ghost method, with a ghost area of 0.005. The two leading jets in the event are excluded in order to remove the hard scattering jets from the background. This approach has been used extensively in jet reconstruction analyses [?, ?]. The corrected jet transverse momentum $p_{T,ch\,jet}^{corr}$ is obtained by subtracting the average background density times the jet area:

$$p_{T,ch\,jet}^{corr} = p_{T,ch\,jet}^{raw} - \rho A_{jet}. \tag{4}$$

For p–Pb collisions a procedure that takes into account sparse environment with the factor $C$, which is the occupancy correction factor, defined as:

$$C = \frac{\sum_j A_j}{A_{\text{acc}}}.$$  (5)

$A_j$ is the area of each $k_T$ jet with at least one real track (i.e. excluding ghosts), $A_{\text{acc}}$ is the area of charged-particle acceptance.

## 8.2 Jet Background Fluctuations

The amount of the jet background fluctuation was evaluated using the Random Cone method. This method consists in generating a random direction in $\eta - \phi$ inside the jet detector acceptance and take all tracks in the event that satisfy $\Delta R < R_{\text{cone}}$ with $R_{\text{cone}}$ equal to the resolution parameter used in the analysis. The raw cone $p_T$ is the sum of the transverse momenta of all particles within the cone. The background fluctuation $\delta p_T$ is calculated as shown in Eq. 6. The distribution is shown in Fig. 14.

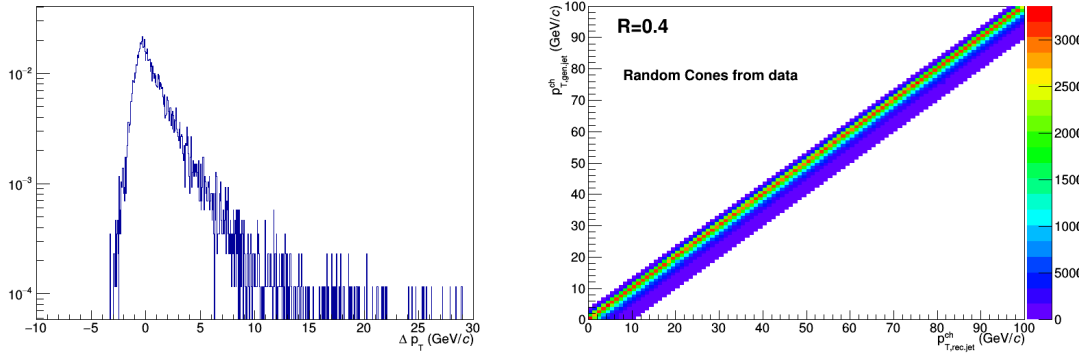$$\delta p_T = p_{T,\text{cone}} - \rho \pi R_{\text{cone}}^2$$  (6)



Fig. 14: Left: $\delta p_T$ distribution obtained with Random Cone method. Right: The background fluctuation matrix built based of the $\delta p_T$ distribution. p–Pb events with $R = 0.4$.

## 9 Feed-Down Correction

A fraction of the measured D mesons originates from the decays of B mesons. These D mesons are usually referred to as non-prompt, to distinguish them from the prompt fraction, i.e. the ones that come directly from the fragmentation of a charm quark or decays of higher excited charm states. The longer decay length of B mesons combined with the topological cuts applied in the D meson selection causes the reconstruction efficiency to be higher for the non-prompt fraction compared to the prompt fraction. This is shown in Fig.Fig. 8. As a consequence, the admixture of the prompt and non-prompt $D - jets$ is biased in a detector-specific way towards the non-prompt. In order to make meaningful comparisons with theoretical and other experimental results one needs to either correct the bias or remove completely the non-prompt fraction and report only the prompt fraction. Both approaches require to use theoretical models or Monte Carlo simulations. In ALICE the second approach has been preferred so far, and for this analysis we decided to follow it.

### 9.1 Monte Carlo Simulation

For the D-meson spectra analysis, ALICE has used FONLL [?] calculations to estimate the non-prompt fraction [?, ?, ?]. In this analysis however we need to extract the B feed-down fraction also as a function

of the jet kinematics, therefore this approach is not applicable. We decided to use POWHEG [?], a Monte Carlo event generator known to reasonably reproduce FONLL calculations and previous experimental results [?]. The second part of the parton shower and the fragmentation into hadrons is provided by PYTHIA6 (Perugia-2011 tune). In addition a boost was applied in order to account for an asymmetric p–Pb collision system.

We generated 25 M $c\bar{c}$ events and 25 M $b\bar{b}$ events for the baseline parameters: $m_c = 1.5$ GeV/$c^2$, $m_b = 4.75$ GeV/$c^2$, $\mu_R = \mu_F = \mu_0 = \sqrt{m^2 + p_T^2}$, where $m_c$ and $m_b$ are repectively the charm and beauty masses, $\mu_R$ and $\mu_F$ are respectively the renormalization and factorization scale factors. Used based PDF set is: CTEQ6 and nPDF: EPS09NLO.

The reconstruction of D-meson jets is performed in the POWHEG+PYTHIA events using the same code employed for the main data analysis.

## 9.2 Feed-Down Subtraction

The B feed-down (FD) is subtracted from the measured D-meson jet $p_T$ spectra by scaling the cross-section of D-meson jets obtained from the analysis of the POWHEG+PYTHIA simulation by the integrated luminosity of the analyzed data, according to Eq. 7:

$$N^{c \to D^{*\pm}}(p_{T,chjet}^{det}) = N^{c,b \to D^{*\pm}}(p_{T,chjet}^{det}) - R_{det}^{b \to D^{*\pm}}(p_{T,chjet}^{det}, p_{T,chjet}^{part}) \otimes \sum_{p_{T,D}} \frac{\varepsilon^{b \to D^{*\pm}}(p_{T,D})}{\varepsilon^{c \to D^{*\pm}}(p_{T,D})} N_{POWHEG}^{b \to D^{*\pm}}(p_{T,D}, p_{T,chjet}^{part}),$$

(7)

where:

- $N^{c \to D^{*\pm}}(p_{T,chjet}^{det})$ is the efficiency-corrected measured yield after FD subtraction;

- $N^{c,b \to D^{*\pm}}(p_{T,chjet}^{det})$ is the efficiency-corrected measured yield before FD subtraction;

- $R_{det}^{b \to D^{*\pm}}(p_{T,chjet}^{det}, p_{T,chjet}^{part})$ is the detector response matrix of the $p_T$ of non-prompt D*±-jets;

- the symbol $\otimes$ is to be interpreted as the standard product of the response matrix times the vector of the yields in bins of $p_{T,chjet}^{part}$;

- $\varepsilon^{c \to D^{*\pm}}(p_{T,D})$ and $\varepsilon^{b \to D^{*\pm}}(p_{T,D})$ are respectively the reconstruction efficiencies of prompt and non-prompt D*± mesons;

- $N_{POWHEG}^{b \to D^{*\pm}}(p_{T,D}, p_{T,chjet}^{part})$ is the cross-section of D*±-jets from the POWHEG simulation scaled by the integrated luminosity of the analyzed data.

The POWHEG D*±-jet spectrum is weighted with the ratio of the prompt over non-prompt efficiency because it is subtracted from the measured yield.

Projections of prompt and non-prompt D*±-jets response matrices in slices $p_{T,chjet}^{part}$ are shown in Fig. 15. There are small differences between the prompt and non-prompt response seen. For this reason the FD has to be subtracted before unfolding the measured spectrum; furthermore, as illustrated in Eq. 7, the spectrum obtained from the POWHEG simulation is smeared using the detector response of non-prompt D*±-jets. Figure 16 compares the measured D*±-jet $p_T$ spectrum with the FD spectrum and the subtracted spectrum.

**MISSING**

Fig. 15: Response matrix in $p_{\mathrm{T,ch\,jet}}^{\mathrm{part}}$ for prompt (red full markers) and non-prompt (open blue markers) $\mathrm{D}^{*\pm}$-jets.

**MISSING**

Fig. 16: Efficiency-corrected measured $\mathrm{D}^{*\pm}$-jet spectrum in p–Pb collisions at $\sqrt{s_{\mathrm{NN}}} = 5.02$ TeV before FD correction (blue full circles) and after FD correction (green full squares). The FD spectrum is also plotted (red open circles).

## 10 Unfolding

Due to detector finite momentum resolution and tracking inefficiency the jet $p_{\mathrm{T}}$ spectra measured as described in the previous sections are distorted. In addition, in p–Pb collisions, fluctuations in the background momentum density introduce additional distortions. These distortions are detector-specific and do not allow a direct comparison with theoretical models and other independent experimental results. An unfolding procedure is employed to correct for these distortions to the best of our knowledge.

In order to correct for these distortions, we first need to assess the detector performance and quantify the detector response to the D-meson jets. In addition, for the p–Pb analysis the background fluctuations are quantified in a fully data-driven fashion.

Figure 17 left shows combined detector and response matrices in p–Pb used for the jet $p_{\mathrm{T}}$ spectra unfolding. The matrix is rebinned according to the binning used for the final jet $p_{\mathrm{T}}$ spectra. Then, the unfolding matrix, a distribution used as a prior and the corrected jet $p_{\mathrm{T}}$ spectrum obtained from the data are passed to the unfolding algorithm. The algorithm returns an unfolded jet $p_{\mathrm{T}}$ spectrum. As a prior, the spectrum obtained from the Monte Carlo simulation at the generator level is used.

**MISSING** **MISSING**

Fig. 17: Left:Combined response matrix calculated with a full simulation of p–Pb events at $\sqrt{s_{\mathrm{NN}}} = 5.02$ TeV. Right:Corrected jet $p_{\mathrm{T}}$ spectrum before (blue) and after (red) the unfolding procedure (Bayesian method with four iterations), p–Pb events at $\sqrt{s_{\mathrm{NN}}} = 5.02$ TeV.

Figure 17 right presents corrected for the reconstruction efficiency and B feed-down jet $p_{\mathrm{T}}$ spectra before the unfolding (blue) and after the unfolding (red), for the side-band method. Unfolding is done with Bayesian and SVD (see 11.3) techniques using the `RooUnfold` software package. The default method is the Bayesian with four iterations.

Comparison of unfolded spectra with different methods and priors is presented in the systematic uncertainties section.

## 11 Systematic Uncertainties

We considered the following sources of systematic uncertainties:

- Raw yield extraction

- B Feed-Down

- Unfolding

- D-Meson Selection Cuts

- Tracking Efficiency

- $p_T$ Shape of the Monte Carlo Spectrum

## 11.1   Raw Yield Extraction

The stability and systematics of the raw yield extraction has been assessed using the `MultiTrial` framework developed by the D2H group. This framework performs the fit of the invariant mass distribution many times varying several conditions, such us binning, fixed vs. free parameters, background function, fit range.

The following variations were included in the assessment of the systematics for the raw yield extraction of D$^{*\pm}$ jets in p–Pb:

  – fixed $\sigma = \sigma_{MC}$;

  – fixed $\sigma = 1.15\sigma_{MC}$

  – fixed $\sigma = 0.85\sigma_{MC}$

  – free $\sigma$ and fixed $m_0 = m_{PDG}$;

  – fixed $\sigma = \sigma_{MC}$ and $m_0 = m_{PDG}$;

  – free $\sigma$ and free $m_0$;

  – background functions: power-law and power-law $\times$ exponential;

  – lower limit of fit range: 0.140, 0.142 GeV/$c^2$;

  – upper limit of fit range: 0.158, 0.160 GeV/$c^2$;

  – rebin by factors 1,2

Figure 18 shows the average of the yields obtained in each of these variations compared with the yields obtained with default fit settings as outlined in Section 5. Both the efficiency-scaled and the side-band method are shown. The systematic uncertainties are calculated as the root-mean-square of all the yields obtained in the multi-trial fits and are shown in Fig. 19.

Figure **??** shows average of the multi-trial procedure for the side-band method as a function of jet $p_T$ for each D$^{*\pm}$ $p_T$ bin scaled by the corresponding efficiency, and average of the all D$^{*\pm}$ $p_T$ bins (blue). And the Fig. **??** presents variations of all considered trials, as a function of jet $p_T$. Variations of all trials as a function of jet $p_T$ for each D$^{*\pm}$ $p_T$ bin and scaled by the corresponding efficiency are shown in Fig 21.
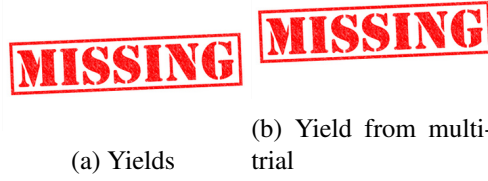
(a) Yields          (b) Yield from multi-trial

Fig. 18: D$^{*\pm}$-jet yields in p–Pb collisions obtained with the efficiency-scaled method (blue) and with the side-band method (red). On the left, the yields are shown with the default fit conditions (full markers) with error bars representing the statistical uncertainty and with the average of the multi-trial fit with filled rectangles representing the RMS of all the multi-trial yields; on the right the results from the multi-trial procedures are depicted.



Fig. 19: The RMS of the multi-trial (systematic uncertainties) is shown for with the efficiency-scaled method (blue) and with the side-band method (red).



Fig. 20: D$^{*\pm}$-jet multi-trial procedure variations in p–Pb collisions obtained with the side-band method. On the left, an average of the multi-trial procedure as a function of jet $p_{\mathrm{T}}$ for each D$^{*\pm}$ $p_{\mathrm{T}}$bin scaled by the corresponding efficiency; Right: variations of all considered trials as a function of jet $p_{\mathrm{T}}$.



Fig. 21: Variations of the trials as a function of jet $p_{\mathrm{T}}$ for each D$^{*\pm}$ $p_{\mathrm{T}}$ bin, scaled by the corresponding efficiency.

## 11.2  B Feed-Down Correction

The B Feed-Down (FD) cross section is obtained from a POWHEG+PYTHIA6 simulation, as discussed in Section 9. In order to assess the systematic uncertainty the same simulation is performed with different choices of the quark mass $m_{\mathrm{b}}$, the factorization scale factor $\mu_{\mathrm{F}}$, the renormalization scale factor $\mu_{\mathrm{S}}$ and the Parton Distribution Functions (PDFs). Table 2 shows the list of parameters used to determine the central points and the variations used to determine the systematic uncertainty.

Figures 22 and 23 compare the cross sections obtained with the various choices of parameters listed in Table 2, respectively as a function of $p_{\mathrm{T,D}}$ and $p_{\mathrm{T,chjet}}$.

Figures 24 shows the final differential cross sections as a function of $p_{\mathrm{T,chjet}}$ with systematic uncertainties. The systematic uncertainties are obtained by taking the largest upward and downward variation

Table 2: Parameters of the POWHEG+PYTHIA6 simulations used to estimate the B Feed-Down.

| Parameter | Central Value | Variations |
|---|---|---|
| $m_b$ | 4.75 GeV/$c^2$ | 4.5, 5.0 GeV/$c^2$ |
| PDF | CTEQ6 (10042) | CT10nlo (11000) |
| nPDF | EPS09nlo | – |
| $(\mu_F, \mu_S)$ | (1,1) | (0.5,0.5), (0.5, 1), (1, 0.5), (2,2), (2,1), (1,2) |

MISSING

Fig. 22: Non-prompt (B Feed-Down) D$^{*\pm}$-jet cross section in p–Pb at $\sqrt{s_{NN}} = 5.02$ TeV as a function of $p_{T,D}$, obtained in POWHEG+PYTHIA6 simulations with different choices of the simulation parameters.

MISSING

Fig. 23: Non-prompt (B Feed-Down) D$^{*\pm}$-jet cross section in p–Pb at $\sqrt{s_{NN}} = 5.02$ TeV as a function of $p_{T,chjet}$, obtained in POWHEG+PYTHIA6 simulations with different choices of the simulation parameters.

from the central point in each bin. In this Figure uncertainties are therefore asymmetric. For the FD subtraction the largest between the upward and downward uncertainty is used in order to have a symmetric uncertainty.

MISSING

Fig. 24: Non-prompt (B Feed-Down) D$^{*\pm}$-jet cross section in p–Pb at $\sqrt{s_{NN}} = 5.02$ TeV, obtained in a POWHEG+PYTHIA6 simulation with the systematic uncertainty.

## 11.3 Unfolding

Figure 25 shows how the unfolded D$^{*\pm}$-jet spectrum in p–Pb collisions evolves with increasing number of iterations, and Fig. 26 presents SVD method [?]. Figure 27 compares the baseline unfolded result (obtained using the Bayesian iterative approach) with the regularized SVD ($k = 6$) method and the bin-by-bin correction method.

Fig. 25: The evolution of the unfolded spectra with increasing number of iterations for the Bayesian method is shown in different colors from 1 to 6 iterations. The ratios between each number-of-iteration choices and the baseline (4 iterations) are shown on the right.



Fig. 26: The evolution of the unfolded spectra with increasing number of iterations for the SVD method is shown in different colors from $k = 3$ to 8. The ratios between each number-of-iteration choices and the baseline ($k = 6$) are shown on the right.



Fig. 27: The ratios between SVD($k = 6$)/Bayesian(four iterations) and bin-by-bin/Bayesian(four iterations).

## 11.4  D-Meson Selection Cuts

## 11.5  Tracking Efficiency

## 11.6  $p_\mathrm{T}$ Shape of the Monte Carlo Spectrum

The $\mathrm{D}^{*\pm}$ reconstruction efficiency is estimated using a PYTHIA6+GEANT3 simulation. A possible source of systematic uncertainty is the $p_\mathrm{T}$ shape of the Monte Carlo spectrum. In order to test the magnitude of this uncertainty we started by comparing the $p_\mathrm{T}$ spectrum obtained from PYTHIA6 with the $p_\mathrm{T}$ spectrum obtained from a POWHEG+PYTHIA6 simulation.

The ratios of the PYTHIA6 spectra over the POWHEG+PYTHIA6 have been fit with a fourth-order polynomial in order to smooth out statistical fluctuations. Then, the fit function of the $p_\mathrm{T,D}$-spectrum ratio has been used to reweigh all the $\mathrm{D}^0$-mesons of the PYTHIA6+GEANT3 simulation. The same weight is applied both at generator level and at detector level in order to probe the sensitivity on the $p_\mathrm{T}$-spectrum shape. The $\mathrm{D}^{*\pm}$ reconstruction efficiency is recalculated in the reweighed simulation.

The effect has been propagated to the raw yields and compared to the default one.

## 11.7  Summary of Systematic Uncertainties

The $p_\mathrm{T}$-independent uncertainties are listed in Table 3. The summary of all uncertainties, including statistical uncertainties are listed for all $p_\mathrm{T,ch\,jet}$ bins of the final spectrum in Table 4.

Table 3: Normalization systematic uncertainties.

| Source | Uncertainty (%) |
|---|---|
| Branching Ratio | |
| Luminosity | |
| Total | |

Table 4: Summary of all uncertainties.

| Source | Uncertainty (%) | | | | | |
|---|---|---|---|---|---|---|
| $p_{\mathrm{T,ch\,jet}}$ (GeV/$c$) | 4 - 6 | 6 - 8 | 8 - 10 | 10 - 16 | 16 - 24 | 24 - 40 |
| Tracking Eff. (Jet Energy Scale) | | | | | | |
| Raw Yield Extraction | | | | | | |
| B Feed-Down | | | | | | |
| Unfolding | | | | | | |
| Selection Cuts | | | | | | |
| Tracking Eff. (D-Meson) | | | | | | |
| Normalization Uncertainty | | | | | | |
| Total Systematic Uncertainty | | | | | | |
| Statistical | | | | | | |
| Total Uncertainty | | | | | | |

## 12 Results

This Section contains a summary of the results. The D$^{*\pm}$-jet $p_{\mathrm{T}}$-differential cross-section in p–Pb collisions at $\sqrt{s_{\mathrm{NN}}} = 5.02$ TeV with all corrections applied (reconstruction efficiency, B feed-down subtraction, unfolding for detector momentum resolution); The cross-section is calculated according to the following formula:

$$\frac{\mathrm{d}^2\sigma}{\mathrm{d}\eta\,\mathrm{d}p_{\mathrm{T}}} = \frac{1}{L_{\mathrm{int}}f_{\mathrm{BR}}}\frac{N_{\mathrm{D-jets}}(p_{\mathrm{T,jet}})}{\Delta p_{\mathrm{T,jet}}\Delta\eta}, \tag{8}$$

where $L_{\mathrm{int}} = N_{\mathrm{evt}}/\sigma_{\mathrm{inel}}$ is the integrated luminosity ($\sigma_{\mathrm{pPb,inel}} = $ b), $f_{\mathrm{BR}}$ is the branching ratio of the D-meson decay channel used in the analysis, $N_{\mathrm{D-jets}}(p_{\mathrm{T,jet}})$ is the measured number of D-jets in a given $p_{\mathrm{T,jet}}$ bin (with all corrections applied).

The D$^{*\pm}$-tagged jet $p_{\mathrm{T}}$ differential cross section in p–Pb collisions at $\sqrt{s_{\mathrm{NN}}} = 5.02$ TeV is shown in Fig.

### 12.1 Monte Carlo Simulations

We performed a set of Monte Carlo simulations using POWHEG and PYTHIA6 to compare with our measurement. The simulations follow the same recipe used for simulating the non-prompt fraction for the B feed-down correction. We simulated 25 M c$\bar{\mathrm{c}}$ events with POWHEG+PYTHIA6 for the central points plus several variations of the parameters of the simulation, listed in Table 5.

Figures 28 and 29 compare the cross sections obtained with the various choices of parameters listed in Table 5, respectively as a function of $p_{\mathrm{T,D}}$ and $p_{\mathrm{T,ch\,jet}}$.

The systematic uncertainties are obtained by taking the largest upward and downward variation.

Table 5: Parameters of the POWHEG+PYTHIA6 simulations of $c\bar{c}$ events used to compare with our measurement.

| Parameter | Central Value | Variations |
|---|---|---|
| $m_b$ | 1.5 GeV/$c^2$ | 1.3, 1.7 GeV/$c^2$ |
| PDF | CTEQ6 (10042) | CT10nlo (11000) |
| nPDF | EPS09nlo | – |
| $(\mu_F, \mu_S)$ | (1,1) | (0.5,0.5), (0.5, 1), (1, 0.5), (2,2), (2,1), (1,2) |



Fig. 28: Prompt D$^{*\pm}$-jet cross section in p–Pb collisions at $\sqrt{s_{NN}} = 5.02$ TeV as a function of $p_{T,D}$, obtained in POWHEG+PYTHIA6 simulations with different choices of the simulation parameters.



Fig. 29: Prompt D$^{*\pm}$-jet cross section in p–Pb collisions at $\sqrt{s_{NN}} = 5.02$ TeV as a function of $p_{T,ch jet}$, obtained in POWHEG+PYTHIA6 simulations with different choices of the simulation parameters.

### 12.1.1 Effect of the $p_{T,D}$ Cut

The effect of the $p_{T,D}$ cut in the D$^{*\pm}$-jet differential cross section has been studied in POWHEG+PYTHIA6.

# 13 Preliminary Figures